BUILDING RESEARCH JOURNAL
VOLUME 60, 2012 NUMBER 3 – 4

ANALYSIS OF INTERFACE CRACK BETWEEN ELASTIC AND PIEZOELECTRIC SOLIDS BY MESHLESS METHOD

SLAVOMÍR KRAHULEC[1], JAN SLADEK[1], VLADIMIR SLADEK[1] AND MICHAEL WÜNSCHE[2]

The paper discusses a crack analysis with the central crack on the interface between elastic and piezoelectric solids under static or dynamic mechanical loading. Due to the specific boundary conditions, the original 3-D crack problem is reduced into a 2-D problem with plane deformation. The crack opening displacements, electric potential and intensity factors are investigated. The intensity factors are computed from the generalized crack-opening-displacements. For the solution of general boundary value problem, the meshless local Petrov-Galerkin (MLPG) method is applied. Here, the local integral equations are derived from the weak form of the governing partial differential equations. Nodal points are uniformly spread on the analyzed domain and each of them is surrounded by a small local circular subdomain. The Heaviside function is used as a test function. On the interface, two sets of nodes are introduced. For the approximation of unknown variables, the Moving Least-Squares (MLS) approximation scheme is used. In the time dependent analysis, the Houbolt finite difference scheme is used. Various electromagnetic boundary conditions are applied on the crack-faces. Two extreme cases are analysed; fully permeable and fully impermeable crack surfaces.

Keywords: the meshless local Petrov-Galerkin (MLPG) method, the Moving Least-Squares (MLS) approximation, the Houbolt finite difference scheme, intensity factors, crack opening displacement

1. Introduction

Recently, piezoelectric materials have been utilized for a wide range of engineering structures. The piezoelectric materials have been frequently used as sensors and actuators for active vibration control of various elastic structures. In this kind of structures, an interface is formed between elastic and piezoelectric material. The material discontinuity in laminated composite materials leads to large interlaminar stresses and the possibility of initiation and propagation of cracks. For this reason, a crack analysis of the interface between two dissimilar materials is important.

The solution of general boundary value problems for coupled problems requires advanced numerical methods due to the high mathematical complexity. The finite element method (FEM) (Enderlein, Ricoeur and Kuna, 2005; Kuna, 2006) and the boundary element method (BEM)

[1] Institute of Construction and Architecture, Slovak Academy of Sciences, Dúbravská cesta 9, 845 03 Bratislava, Slovak Republic, e-mail: slavomir.krahulec@savba.sk, jan.sladek@savba.sk, vladimir.sladek@savba.sk
[2] Department of Civil Engineering, University of Siegen, D-57068 Siegen, Germany

(Pan, 1999; García-Sánchez, Zhang and Sáez, 2008) have been applied for crack analyses in homogeneous piezoelectric solids. The FEM is well established and often used for the solution of general boundary value problems. In the last two decades, modelling piezoelectric materials using the FEM was one of the most active research topics. The BEM is an alternative method to the FEM. This method is an effective and convenient numerical tool, but there are still certain restrictions such as need for a fundamental solution. It is desirable to develop new advanced methods. One of these are meshless methods, which are becoming popular due to their advantages in higher adaptivity and lower cost in preparing input data for a numerical analysis. The meshless methods can be based on a weak-form formulation over the global domain or by setting of local subdomains. In the global formulation, background cells are required for the integration of the weak-form. In the methods based on the local weak-form formulation, no background cells are required and therefore they are called as the truly meshless methods. Various types of meshless method have been applied to piezoelectric problems (Sladek, Sladek, Stanak, Zhang and Wünsche, 2013; Chen, Li, Liu and Xue, 2013; Stanak, Sladek, Sladek and Krahulec, 2012; Yin and Yao, 2012; Ohs and Aluru, 2001). The present paper uses the meshless local Petrov-Galerkin (MLPG) method. The method is based on the local weak-form formulation, in which trial and test functions can be chosen from different functional spaces. The MLPG method has been applied for the crack analysis of piezoelectric material in continuously nonhomogeneous solids (Sladek, Sladek, Zhang, Solek and Starek, 2007; Sladek, Sladek, Zhang, Solek and Pan, 2007) as well as for the investigation of central cracks on the interface between two dissimilar piezoelectric solids (Sladek, Sladek, Wunsche and Zhang, 2012).

The present paper discusses the analysis of an interface crack between elastic and piezoelectric solids. A finite strip with the central crack is considered. The upper face of the crack belongs to the piezoelectric solid and the lower face to the elastic solid. The meshless local Petrov-Galerkin (MLPG) method is applied to solve the boundary value problem. As a special variant of the MLPG, the local integral equations are derived from the governing partial differential equations applying a Heaviside step function as the test functions in the weak-form. Nodal points are spread on the analyzed domain and each of them is surrounded by a small local subdomain. For simplicity, the shape of local subdomain is circle. The Moving Least-Squares (MLS) approximation is used to approximate the spatial variations of the displacements and electric potentials. By joining two dissimilar materials, a discontinuity is caused on the interface. Therefore, double nodes are introduced at the material discontinuity. Two set of nodes are placed on the material interface at the same location, but with different material properties. In the time dependent analysis, the Houbolt finite difference scheme is used. The crack opening displacements, electric potentials, stress intensity factors and electrical displacement intensity factors are investigated. The FEM results obtained by the commercial code COMSOL Multiphysics are used as a benchmark solution.

2. Basic equations of piezoelectricity

The basic equations of linear piezoelectric materials consist of the constitutive equations and governing equations. The coupling of the mechanical and electrical fields in piezoelectric solids (Tiersten, 1969) is given by the following constitutive equations

$$\sigma_{ij}(\mathbf{x},t) = c_{ijkl}(\mathbf{x})\varepsilon_{kl}(\mathbf{x},t) - e_{kij}(\mathbf{x})E_k(\mathbf{x},t), \tag{1}$$

$$D_j(\mathbf{x},t) = e_{jkl}(\mathbf{x})\varepsilon_{kl}(\mathbf{x},t) + h_{jk}(\mathbf{x})E_k(\mathbf{x},t), \tag{2}$$

where σ_{ij} and D_j represent the stress tensor and the electric displacements, respectively. Material parameters are the elastic coefficients c_{ijkl}, dielectric constants h_{jk} and the coefficients for the piezoelectric coupling e_{kij}. The strain tensor ε_{kl} and electric field vector E_k are expressed in terms of derivatives of displacements u_i and electrical potential ψ by

$$\varepsilon_{ij}(\mathbf{x},t) = \frac{1}{2}\left(u_{i,j}(\mathbf{x},t) + u_{j,i}(\mathbf{x},t)\right), \tag{3}$$

$$E_k(\mathbf{x},t) = -\psi_{,k}(\mathbf{x},t) \tag{4}$$

In this paper, a two layered composite is considered, which consists of a piezoelectric and elastic layer.

It should be mentioned, that the piezoelectric constants e_{ijk} vanish for the elastic layer and therefore Eq. (1) and (2) are uncoupled.

The original 3-D crack problem is reduced into a 2-D problem with plane deformation. Therefore, the constitutive equations (1) – (2) can be written in a matrix form (Parton and Kudryavtsev, 1988)

$$\begin{bmatrix}\sigma_{11}\\ \sigma_{33}\\ \sigma_{13}\end{bmatrix} = \begin{bmatrix}c_{11} & c_{13} & 0\\ c_{13} & c_{33} & 0\\ 0 & 0 & c_{44}\end{bmatrix}\begin{bmatrix}\varepsilon_{11}\\ \varepsilon_{33}\\ 2\varepsilon_{13}\end{bmatrix} - \begin{bmatrix}0 & e_{31}\\ 0 & e_{33}\\ e_{15} & 0\end{bmatrix}\begin{bmatrix}E_1\\ E_3\end{bmatrix} = \mathbf{C}(\mathbf{x})\begin{bmatrix}u_{1,1}\\ u_{3,3}\\ u_{1,3}+u_{3,1}\end{bmatrix} - \mathbf{L}(\mathbf{x})\begin{bmatrix}-\psi_{,1}\\ -\psi_{,3}\end{bmatrix}, \tag{5}$$

$$\begin{bmatrix}D_1\\ D_3\end{bmatrix} = \begin{bmatrix}0 & 0 & e_{15}\\ e_{31} & e_{33} & 0\end{bmatrix}\begin{bmatrix}\varepsilon_{11}\\ \varepsilon_{33}\\ 2\varepsilon_{13}\end{bmatrix} + \begin{bmatrix}h_{11} & 0\\ 0 & h_{33}\end{bmatrix}\begin{bmatrix}E_1\\ E_3\end{bmatrix} = \mathbf{G}(\mathbf{x})\begin{bmatrix}u_{1,1}\\ u_{3,3}\\ u_{1,3}+u_{3,1}\end{bmatrix} + \mathbf{H}(\mathbf{x})\begin{bmatrix}-\psi_{,1}\\ -\psi_{,3}\end{bmatrix}. \tag{6}$$

Governing equations for piezoelectric body are given by the balance of momentum and the scalar Maxwell's equation as

$$\sigma_{ij,j}(\mathbf{x},t) + X_i(\mathbf{x},t) = \rho\ddot{u}_i(\mathbf{x},t), \tag{7}$$

$$D_{j,j}(\mathbf{x},t) - \Pi(\mathbf{x},t) = 0, \tag{8}$$

where $\ddot{u}_i$, ρ, X_i and Π represent the acceleration of the displacement, the mass density, the body force vector and the volume density of free charges, respectively. In case of static loading conditions, the right hand side of equation (7) is equal to zero.

On a portion of the global boundary $\partial\Omega$, the Dirichlet boundary conditions for the mechanical displacements and the electric potential are assumed as follows

$$\begin{aligned} u_i(\mathbf{x},t) &= \tilde{u}_i(\mathbf{x},t), \quad \text{on} \quad \partial\Omega_u,\\ \psi(\mathbf{x},t) &= \tilde{\psi}(\mathbf{x},t), \quad \text{on} \quad \partial\Omega_\psi, \end{aligned} \tag{9}$$

while the Neumann boundary conditions for the traction vector and the normal component of the electric displacement vector on the rest of the boundary are given by

$$\begin{aligned} T_i(\mathbf{x},t) &= \sigma_{ij}(\mathbf{x},t)n_j(\mathbf{x}) = \tilde{T}_i(\mathbf{x},t), \quad \text{on} \quad \partial\Omega_t, \partial\Omega = \partial\Omega_u \cup \partial\Omega_t, \\ Q(\mathbf{x},t) &= D_i(\mathbf{x},t)n_i(\mathbf{x}) = -\tilde{Q}(\mathbf{x},t), \quad \text{on} \quad \partial\Omega_q, \partial\Omega = \partial\Omega_v \cup \partial\Omega_q, \end{aligned} \tag{10}$$

where $\tilde{u}_i$, $\tilde{\psi}$, $\tilde{T}_i$ and $\tilde{Q}$ are prescribed variables for the mechanical displacements, the electric potential, the traction vector and the electric displacement vector on the parts of the global boundary $\partial\Omega_u$, $\partial\Omega_v$, $\partial\Omega_t$ and $\partial\Omega_q$, respectively and n_i is the unit outward normal vector.

In this paper, two extreme boundary conditions on crack faces are considered; the fully impermeable and fully permeable conditions. The electrical boundary condition on crack faces along x_1 for fully impermeable case is given as

$$D_3(\mathbf{x} \in \partial\Omega_c^+, t) = D_3(\mathbf{x} \in \partial\Omega_c^-, t) = 0, \tag{11}$$

where $\partial\Omega_c^+$ and $\partial\Omega_c^-$ are the upper and the lower crack faces, respectively.

The fully permeable crack face boundary condition along x_1 is given by

$$D_3(\mathbf{x} \in \partial\Omega_c^+, t) = D_3(\mathbf{x} \in \partial\Omega_c^-, t), \tag{12}$$

$$\psi(\mathbf{x} \in \partial\Omega_c^+, t) - \psi(\mathbf{x} \in \partial\Omega_c^-, t) = 0. \tag{13}$$

3. Local integral equation and meshless implementation

The MLPG method constructs a weak-form over the local fictitious subdomains such as Ω_s (Fig. 1), which is a small region taken around each node inside the global domain (Atluri, 2004).

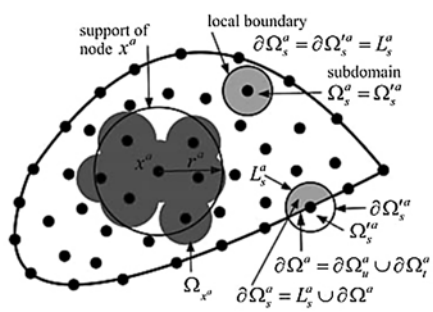

Figure 1. Local boundaries for weak formulation, the domain Ω_x^a for MLS approximation of the trial function and the support area of weight function around node x^a

The local weak form for governing equations (7) – (8) is given as follows

$$\int_{\Omega_s} [\sigma_{ij,j}(\mathbf{x},t) + X_i(\mathbf{x},t) - \rho(\mathbf{x})\ddot{u}_i(\mathbf{x},t)]u_{ik}^*(\mathbf{x})d\Omega = 0\,, \tag{14}$$

$$\int_{\Omega_s} [D_{j,j}(\mathbf{x},t) - \Pi(\mathbf{x},t)]\psi^*(\mathbf{x})d\Omega = 0\,, \tag{15}$$

where the superscript star is used for test functions. In this paper, the Heaviside test function is used, in which it is valid

$$u_{ik}^*(\mathbf{x}) = \begin{cases} \delta_{ik} & \text{at} \quad \mathbf{x} \in (\Omega_s \cup \partial\Omega_s) \\ 0 & \text{at} \quad \mathbf{x} \notin (\Omega_s \cup \partial\Omega_s) \end{cases}, \tag{16}$$

$$\psi^*(\mathbf{x}) = \begin{cases} 1 & \text{at} \quad \mathbf{x} \in (\Omega_s \cup \partial\Omega_s) \\ 0 & \text{at} \quad \mathbf{x} \notin (\Omega_s \cup \partial\Omega_s) \end{cases}. \tag{17}$$

By using the Heaviside functions as the test function (16) – (17) and applying the Gauss divergence theorem to equations (14) – (15), one obtains the following local boundary-domain integral equations

$$\int_{L_s+\Gamma_{su}} T_i(\mathbf{x},t)d\Gamma + \int_{\Gamma_{st}} \tilde{T}_i(\mathbf{x},t)d\Gamma + \int_{\Omega_s} X_i(\mathbf{x},t)d\Omega - \int_{\Omega_s} \rho(\mathbf{x})\ddot{u}_i(\mathbf{x},t)d\Omega = 0\,, \tag{18}$$

$$\int_{L_s+\Gamma_{sw}} Q(\mathbf{x},t)d\Gamma - \int_{\Gamma_{sq}} \tilde{Q}(\mathbf{x},t)d\Gamma - \int_{\Omega_s} \Pi(\mathbf{x},t)d\Omega = 0\,. \tag{19}$$

For the trial functions, the MLS-approximation is employed. According to the MLS method (Belytschko, Krongauz, Organ, Fleming and Krysl, 1996), the approximation of displacement and electric potential fields and their derivatives is given as

$$\mathbf{u}^h(\mathbf{x},t) = \sum_{a=1}^{n} \phi^a(\mathbf{x})\hat{\mathbf{u}}^a(t)\,, \quad \mathbf{u}_{,l}^h(\mathbf{x},t) = \sum_{a=1}^{n} \phi_{,l}^a(\mathbf{x})\hat{\mathbf{u}}^a(t)\,, \tag{20}$$

$$\psi^h(\mathbf{x},t) = \sum_{a=1}^{n} \phi^a(\mathbf{x})\hat{\psi}^a(t)\,, \quad \psi_{,l}^h(\mathbf{x},t) = \sum_{a=1}^{n} \phi_{,l}^a(\mathbf{x})\hat{\psi}^a(t)\,, \tag{21}$$

where the nodal values $\hat{\mathbf{u}}^a = \left(\hat{u}_1^a, \hat{u}_3^a\right)^T$ and $\hat{\psi}^a$ are fictitious parameters for the displacements and the electric potentials, respectively, and $\phi^a(\mathbf{x})$ is the shape function associated with the node *a*. Number of nodes *n* is specified by the nonzero weight function appearing in the definition of MLS shape function through the radius of support domain (Fig. 1) (Atluri, 2004). In this paper, a spline

function of the fourth-order is used as the weight function, which guaranties C^1 continuity over the analyzed domain. It is seen that the C^1 continuity is ensured over the entire domain, and therefore the continuity conditions of the tractions and electric displacements are satisfied. However, this highly continuous nature leads to difficulties when there is an imposed discontinuity in the secondary fields (strains and electric field vector). Therefore, the double nodes are introduced at the interface of layers, one for each layer with proper material properties (Fig. 2) (Sladek, Sladek, Wünsche and Zhang, 2009). For these nodes, it is important to ensure the continuity of the displacements, the electric potential and the normal component of the electric displacement vector as well as the equilibrium of the tractions by coupling conditions as follows

$$u_i^+(\mathbf{x},t)=u_i^-(\mathbf{x},t)\,,\quad T_i^+(\mathbf{x},t)+T_i^-(\mathbf{x},t)=0\,, \tag{22}$$

$$\psi^+(\mathbf{x},t)=\psi^-(\mathbf{x},t)\,,\quad Q^+(\mathbf{x},t)+Q^-(\mathbf{x},t)=0\,. \tag{23}$$

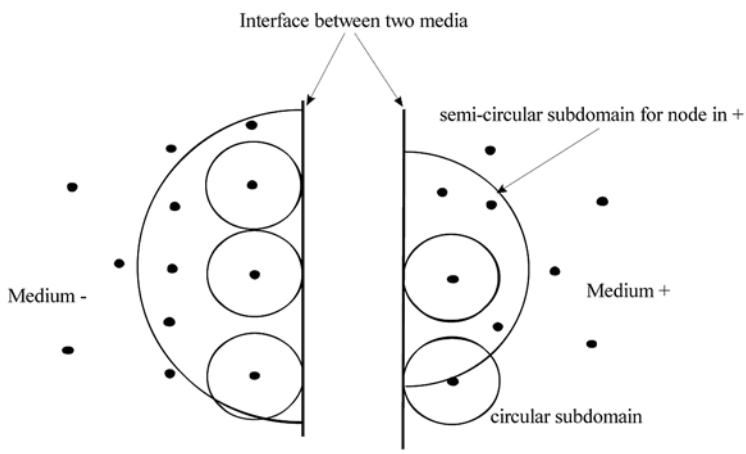

Figure 2. Modelling of material discontinuities

Substitution of (20) – (21) into the constitutive relations (1) – (2) and subsequently into the local integral equations (18) – (19) leads to the discretized local integral equations

$$\sum_{a=1}^{n}\left(\int_{L_s+\partial\Omega_{st}}\mathbf{N}(\mathbf{x})\mathbf{C}(\mathbf{x})\mathbf{B}^a(\mathbf{x})d\Gamma\right)\hat{\mathbf{u}}^a+\sum_{a=1}^{n}\left(\int_{L_s+\partial\Omega_{st}}\mathbf{N}(\mathbf{x})\mathbf{L}(\mathbf{x})\mathbf{P}^a(\mathbf{x})d\Gamma\right)\hat{\psi}^a$$
$$-\sum_{a=1}^{n}\left(\int_{\Omega_s}\rho(\mathbf{x})\phi^a(\mathbf{x})d\Omega\right)\ddot{\hat{\mathbf{u}}}^a(t)=-\int_{\partial\Omega_{st}}\tilde{\mathbf{T}}(\mathbf{x})d\Gamma-\int_{\Omega_s}\mathbf{X}(\mathbf{x})d\Omega\,, \tag{24}$$

$$\sum_{a=1}^{n}\left(\int_{L_s+\partial\Omega_{sq}}\mathbf{n}(\mathbf{x})\mathbf{G}(\mathbf{x})\mathbf{B}^a(\mathbf{x})d\Gamma\right)\hat{\mathbf{u}}^a - \sum_{a=1}^{n}\left(\int_{L_s+\partial\Omega_{sq}}\mathbf{n}(\mathbf{x})\mathbf{H}(\mathbf{x})\mathbf{P}^a(\mathbf{x})d\Gamma\right)\hat{\psi}^a(t) = \int_{\partial\Omega_{sq}}\tilde{Q}(\mathbf{x},\tau)d\Gamma + \int_{\Omega_s}\Pi(\mathbf{x},t)d\Omega\ , \tag{25}$$

which are applied on the subdomains adjacent to the interior nodes as well as to the boundary nodes on $\partial\Omega_{st}$ and $\partial\Omega_{sq}$. The matrices $\mathbf{C}(\mathbf{x})$, $\mathbf{L}(\mathbf{x})$, $\mathbf{G}(\mathbf{x})$, and $\mathbf{H}(\mathbf{x})$ are defined in constitutive equations (6) – (7) and the matrix $\mathbf{N}(\mathbf{x})$ is related to the normal vector $\mathbf{n}(\mathbf{x})$ on $\partial\Omega_s$ by

$$\mathbf{N}(\mathbf{x}) = \begin{bmatrix} n_1 & 0 & n_3 \\ 0 & n_3 & n_1 \end{bmatrix} \tag{26}$$

and finally, the matrices $\mathbf{B}^a$ and $\mathbf{P}^a$ are represented by the gradients of the shape functions as

$$\mathbf{B}^a(\mathbf{x}) = \begin{bmatrix} \phi^a_{,1} & 0 \\ 0 & \phi^a_{,3} \\ \phi^a_{,3} & \phi^a_{,1} \end{bmatrix}, \quad \mathbf{P}^a(\mathbf{x}) = \begin{bmatrix} \phi^a_{,1} \\ \phi^a_{,3} \end{bmatrix}. \tag{27}$$

A collocation approach is used to impose Dirichlet boundary conditions directly, using MLS variable approximation (20) – (21).

Collecting the discretized local boundary-domain integral equations (24) – (25) together with the discretized boundary conditions for the displacements and the electrical potential and the interface conditions (22) – (23), we get a complete system of ordinary differential equations,

$$\mathbf{M}\ddot{\mathbf{x}} + \mathbf{K}\mathbf{x} = \mathbf{F}\ , \tag{28}$$

where $\mathbf{K}$ is the stiffness matrix of the structure, $\mathbf{M}$ is the mass matrix, $\mathbf{F}$ is the loading vector and $\mathbf{x}$ is the vector of unknown quantities, defined as $\mathbf{x} = [\hat{u}_1^a, \hat{u}_3^a, \hat{\psi}^a]^T$.

Explicit method, such as Houbolt finite difference scheme (Houbolt, 1950), which uses the differential equation at time t to predict a solution at time $t + \Delta t$ can be used. In the method, the acceleration $\ddot{\mathbf{x}}$ is expressed as

$$\ddot{\mathbf{x}}_{t+\Delta t} = \frac{2\mathbf{x}_{t+\Delta t} - 5\mathbf{x}_t + 4\mathbf{x}_{t-\Delta t} - \mathbf{x}_{t-2\Delta t}}{\Delta t^2}\ , \tag{29}$$

where Δt is the time-step.

Substituting Eq. (29) into Eq. (28), the following system of algebraic equations for the unknowns $\mathbf{x}_{t+\Delta t}$ it is obtained

$$\left[\frac{2}{\Delta t^2}\mathbf{M}+\mathbf{K}\right]\mathbf{x}_{t+\Delta t}=\frac{1}{\Delta t^2}5\mathbf{M}\mathbf{x}_t+\mathbf{M}\frac{1}{\Delta t^2}\left\{-4\mathbf{x}_{t-\Delta t}+\mathbf{x}_{t-2\Delta t}\right\}+\mathbf{F}\,. \tag{30}$$

4. Intensity factors

The generalized crack-opening-displacements $\Delta\mathbf{u} = [u_1, u_3, \psi]^T$ for an interface crack between two dissimilar piezoelectric layers have been derived by Suo et al. (Suo, Kuo, Barnett and Willis, 1992) with

$$\Delta\mathbf{u}(r)=(\mathbf{H}+\bar{\mathbf{H}})\sqrt{\frac{r}{2\pi}}\left[\frac{Kr^{i\varepsilon_1}\mathbf{w}}{(1+2i\varepsilon_1)\cosh(\pi\varepsilon_1)}+\frac{\bar{K}r^{-i\varepsilon_1}\bar{\mathbf{w}}}{(1-2i\varepsilon_1)\cosh(\pi\varepsilon_1)}+\frac{K_4r^{-\varepsilon_2}\mathbf{w}_4}{(1-2\varepsilon_2)\cosh(\pi\varepsilon_2)}\right], \tag{31}$$

where $K = K_1 + iK_2$ is the complex stress intensity factor, K_4 is the electric displacement intensity factor, an overbar denotes the complex conjugate and r is the distance from the crack-tip to measured data. The complex Hermitian matrix $\mathbf{H}$ is determined by the material properties from the both layers and computed from the eigenvalue problem as shown in (Wünsche, Zhang, Sladek, Sladek, Hirose and Kuna, 2009). The bimaterial constants ε_1 and ε_2 as well as the eigenvectors $\mathbf{w}$ and $\mathbf{w}_4$ are determined by the eigenvalue problem

$$\mathbf{D}^{-1}\mathbf{W}\mathbf{w}=-i\beta\mathbf{w}\,, \tag{32}$$

with $\mathbf{H} = \mathbf{D} + i\mathbf{W}$. The eigenvalue β is either real or purely imaginary and related to the bimaterial constants by

$$\varepsilon_1=\frac{1}{2}\ln\frac{1-\beta}{1+\beta},\quad \varepsilon_2=\frac{1}{2}\ln\frac{1-i\beta}{1+i\beta}\,. \tag{33}$$

Eq. (33) is consistent for the interface crack between a piezoelectric and a non-piezoelectric anisotropic layer, as investigated in the present work and therefore the computation of the intensity factors can be performed as shown in Sladek, Sladek, Wünsche and Zhang (2012).

5. Numerical examples and results

As a numerical example a composite strip under the pure mechanical load $\sigma_0 = 10^4$ in the x_3-direction is analyzed (Fig. 3).

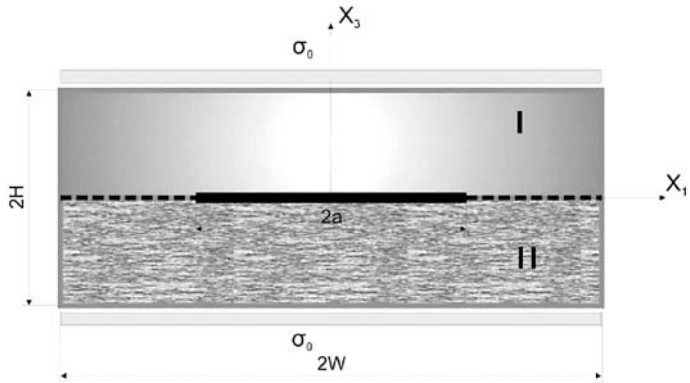

Figure 3. Geometry of the composite strip with central crack and mechanical load

The strip consists of piezoelectric layer at the top and elastic layer at the bottom with material parameters shown in Table1. The central crack on the interface of two dissimilar materials is considered. The problem can be solved as a 2-D problem under plane deformation conditions due to the considered boundary conditions. The width of the strip is $w = 0.1m$ and height of each layer is $h_I = h_{II} = 0.04m$. The crack with length $a = 0.05m$ along the axis x_1 is assumed.

Table 1. Material properties of considered materials

	I (PZT4)	**II (graphite/epoxy)**
$\mathbf{c_{11}}$ **(Nm^{-2})**	13.9 x 10^{10}	13.53 x 10^{10}
$\mathbf{c_{13}}$ **(Nm^{-2})**	7.43 x 10^{10}	0.516 x 10^{10}
$\mathbf{c_{33}}$ **(Nm^{-2})**	11.5 x 10^{10}	1.436 x 10^{10}
$\mathbf{c_{44}}$ **(Nm^{-2})**	2.6 x 10^{10}	0.565 x 10^{10}
$\mathbf{h_{11}}$ **(C(Vm)$^{-1}$)**	6.46 x 10^{-9}	3*6.46 x 10^{-9}
$\mathbf{h_{33}}$ **(C(Vm)$^{-1}$)**	5.62 x 10^{-9}	3*5.62 x 10^{-9}
$\mathbf{e_{31}}$ **(Cm^{-2})**	-5.2	0
$\mathbf{e_{33}}$ **(Cm^{-2})**	15.1	0
$\mathbf{e_{15}}$ **(Cm^{-2})**	12.7	0
ρ(kgm^{-3})	7500	1578

For the analysis, only half of the strip is needed due to symmetry around the axis x_3. In the MLPG method, we used 630 (2 x 21 x 15) nodes equidistantly distributed (Fig. 4) and circular local subdomains with the radius $r_{loc} = 0.0023m$. For mesh in the finite element method, we used 1 600 (2 x 32 x 25) quadratic elements.

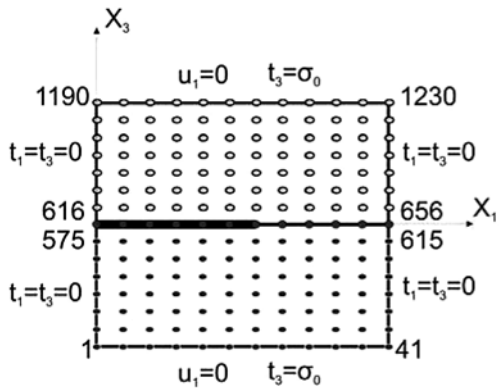

Figure 4. Node distribution and boundary conditions

In the numerical computations, impermeable or permeable electrical boundary conditions on the crack-face are considered; therefore vanishing electrical displacements or electrical potential according with equations (12) – (14) are prescribed, respectively.

In the first set of results, a static tensile load is considered. The results shown in Figures 5 – 7 correspond to two different electrical boundary conditions on the crack faces. A good agreement between results obtained by the MLPG and the finite element method is observed. An asymmetry is observed between $|u_3|$ at the top and bottom crack faces due to different stiffness parameters. Further, one can see larger crack opening displacement in the case with permeable boundary condition.

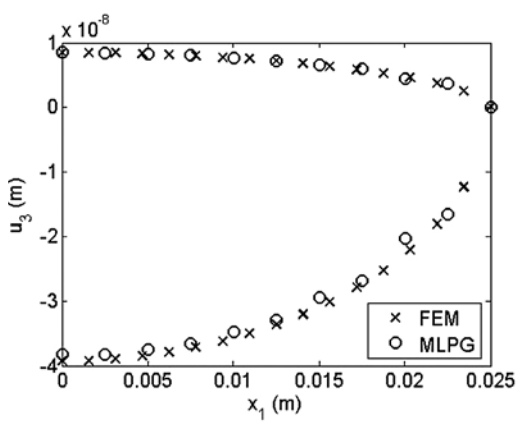

Figure 5. The crack displacement with the permeable condition and a static loading

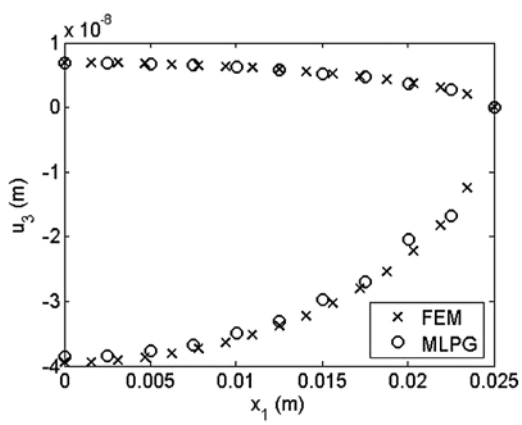

Figure 6. The crack displacement with the impermeable condition and a static loading

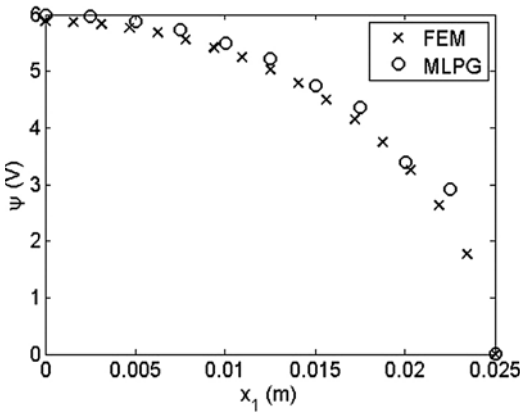

Figure 7. The electrical potential on the crack faces with the impermeable condition and a static loading

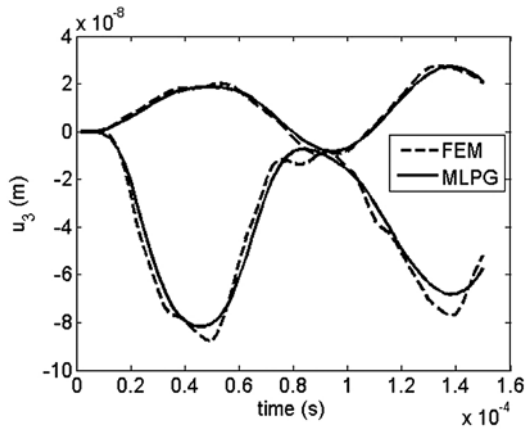

Figure 8. The crack displacement with the permeable condition and a dynamic loading

In the next numerical examples, the same strip is subjected to a pure mechanical impact loading $\sigma_3(t) = \sigma_0 H(t)$. In the numerical computations a time-step $\Delta t = 2.5\mu s$ is used. The crack opening displacements in the centre of the crack faces (x_1=0) are shown in Figures 8 – 10. Again, there is a good agreement between results obtained by the MLPG and finite element method in Figures 8 – 9. On the contrary to the static case, the results approximately demonstrate double increase. In the comparison of both electric boundary conditions shown in Figure 9, one can also observe the larger crack opening displacement in the case of the permeable boundary condition.

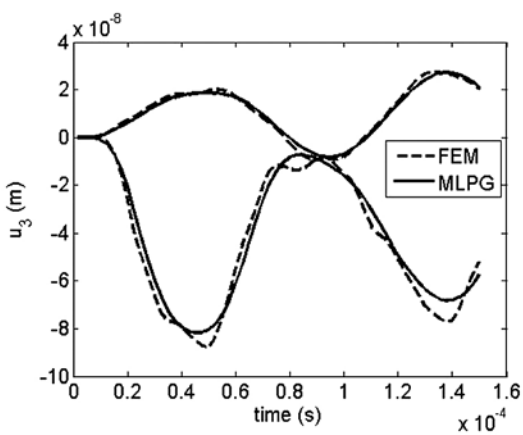

Figure 9. The crack displacement with the impermeable condition and a dynamic loading

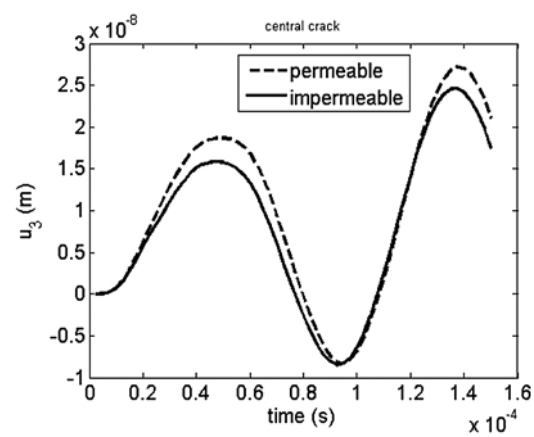

Figure 10. Influence of the electric boundary condition on the crack displacement under a dynamic load

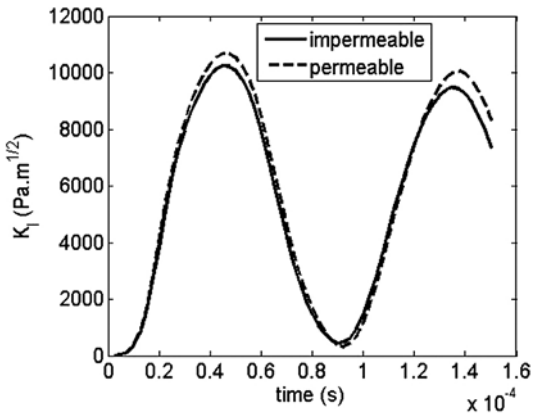

Figure 11. Mode-I stress intensity factors in a strip under a dynamic load

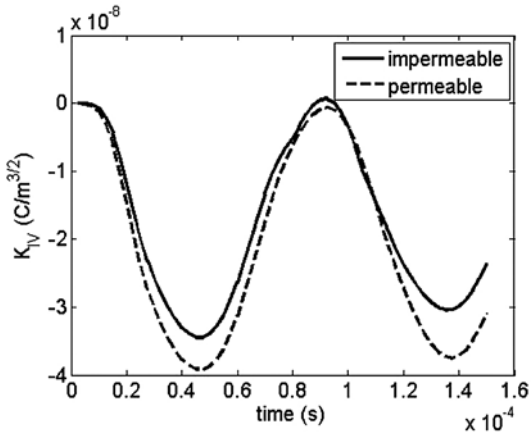

Figure 12. Electrical displacement intensity factors in a strip under a dynamic load

Finally, the influence of the electrical boundary conditions on the intensity factors is analyzed. For both electrical boundary conditions on the crack-faces in the static analysis, the stress intensity factor (SIF) $K_1 = 5.37\times10^3\ Pam^{1/2}$ for permeable and $K_1 = 5.13\times10^3\ Pam^{1/2}$ for impermeable boundary conditions are very similar. The almost vanishing electrical displacement intensity factor (EDIF) is observed as $K_4 = 1.97\times10^{-8}\ Cm^{-3/2}$ for permeable and $K_4 = 1.70\times10^{-8}\ Cm^{-3/2}$ for impermeable boundary conditions. In case of a pure mechanical load, one can observe a finite value of the electrical potential, while EDIF is vanishing. The maximum dynamic SIFs are larger than their corresponding static values. In the investigated example this 'dynamic overshoot' has the factor two.

6. Conclusion

The 2-D interface central crack problem between two dissimilar solids was analyzed by meshless local Petrov-Galerkin method (MLPG). A piezoelectric layer at the top and a graphite/epoxy at the bottom of the strip were considered. Both impermeable and permeable electrical boundary conditions on the crack-faces were considered. Numerical results for static and dynamic crack analysis were presented.

The numerical results indicate a significant influence of the electrical crack face boundary conditions on the electrical intensity factor under a pure mechanical load. A small influence is observed for the stress intensity factor.

REFERENCES

[1] Atluri, S. N. (2004), The Meshless Method, (MLPG) For Domain & BIE Discretizations, Forsyth: Tech Science Press.

[2] Belytschko, T. B., Krongauz, Y., Organ, D. J., Fleming, M. and Krysl, P. (1996), "Meshless methods: An overview and recent developments", *Computer Methods in Applied Mechanics and Engineering* 1-4, 3-47.

[3] Chen, S. S., Li, H. Q., Liu, H. Y. and Xue, Z. Q. (2013), "A meshless local natural neighbour interpolation method for analysis of two-dimensional piezoelectric structures", *Engineering Analysis with Boundary Elements,* sv. 37, 2, 273-279.

[4] Enderlein, M., Ricoeur, A. and Kuna, M. (2005), "Finite element techniques for dynamic crack analysis in piezoelectrics", *International Journal of Fracture* 3-4, 191-208.

[5] García-Sánchez, F., Zhang, C. and Sáez, A. (2008), "2-D transient dynamic analysis of cracked piezoelectric solids by a time-domain BEM", *Computer Methods in Applied Mechanics and Engineering* 33-40, 3108-3121.

[6] Houbolt, J. C. (1950), "A recurrence matrix solution for the dynamic response of elastic aircraft", *Journal of Aeronautical Sciences*, 371-376.

[7] Kuna, M. (2006), „Finite element analyses of cracks in piezoelectric structures: A survey", *Archive of Applied Mechanics,* sv. 76, 11-12, 725-745.

[8] Ohs, R. R. and Aluru, N. R. (2001), "Meshless analysis of piezoelectric devices", *Computational Mechanics* 1, 23-36.

[9] Pan, E. (1999), "A BEM analysis of fracture mechanics in 2D anisotropic piezoelectric solids", *Engineering Analysis with Boundary Elements* 1, 67-76.

[10] Parton, V. Z. and Kudryavtsev, B. A. Electromagnetoelasticity, Piezoelectrics and Electrically Conductive Solids, New York: Gordon and Breach Science Publishers, 1988.

[11] Sladek, J., Sladek, V., Stanak, P., Zhang, C. and Wünsche, M. (2013), "Analysis of the bending of circular piezoelectric plates with functionally graded material properties by a MLPG method," *Engineering Structures,* vol. 47, 81-89.

[12] Sladek, J., Sladek, V., Wünsche, M. and Zhang, C. (2012), "Analysis of an interface crack between two dissimilar piezoelectric solids", *Engineering Fracture Mechanics,* vol. 89, 114–127.

[13] Sladek, J., Sladek, V., Wünsche, M. and Zhang, C. (2009) „Interface crack problems in anisotropic solids analyzed by the MLPG", *CMES - Computer Modeling in Engineering & Sciences,* sv. 54, 223-252.

[14] Sladek, J., Sladek, V., Zhang, C. Solek, P. and Pan, E. (2007), "Evaluation of fracture parameters in continuously nonhomogeneous piezoelectric solids", *International Journal of Fracture* 4, 313-326.

[15] Sladek, J., Sladek, V., Zhang, C., Solek, P. and Starek, L. (2007), "Fracture analyses in continuously nonhomogeneous piezoelectric solids by the MLP", *CMES: Computer Modeling in Engineering & Sciences* 3, 247-262.

[16] Stanak, P., Sladek, J., Sladek, V. and Krahulec, S. (2012), "Meshless analysis of circular plate with varying position of piezoactuator", in *ECCOMAS 2012 - European Congress on Computational Methods in Applied Sciences and Engineering, e-Book Full Papers*, Vienna.

[17] Suo, Z., Kuo, C. M., Barnett, D. M. and Willis, J. R. (1992), "Fracture mechanics for piezoelectric ceramics", *Journal of the Mechanics and Physics of Solids* 4, 739-765.

[18] Tiersten, H. F. (1969), Linear piezoelectric plate vibration, New York: Plenum Press.

[19] Wünsche, M. Zhang, C. Sladek, J. Sladek, V., Hirose, S. and Kuna, M. (2009), "Transient dynamic analysis of interface cracks in layered anisotropic solids under impact loading", *International Journal of Fracture* 1-2, 131-147.

[20] Yin, Y. a Yao, Q. L. (2012), "Analysis of piezoelectric laminated plates using the layerwise plate theory and radial basis function collocation method", v *Proceedings of the 2012 Symposium on Piezoelectricity, Acoustic Waves and Device Applications, SPAWDA 2012Proceedings of the 2012 Symposium on Piezoelectricity, Acoustic Waves and Device Applications, SPAWDA 2012*, Shanghai.